AlGaAs emitter/GaAs barrier terahertz detector with a 2.3 THz threshold

M. B. M. Rinzan and A. G. U. Perera[a)]
Department of Physics and Astronomy, Georgia State University, Atlanta, Georgia 30303

S. G. Matsik
NDP Optronics LLC, 236 St. Martins Drive, Mableton, Georgia 30126

H. C. Liu, Z. R. Wasilewski, and M. Buchanan
Institute for Microstructural Sciences, National Research Council, Ottawa K1A 0R6, Canada

(Received 18 November 2004; accepted 22 December 2004; published online 9 February 2005)

A heterojunction interfacial work function internal photoemission (HEIWIP) detector with a threshold frequency (f_0) of 2.3 THz ($\lambda_0=128\ \mu$m) is demonstrated. The threshold limit of ~3.3 THz (92 μm) due to the Al fraction being limited to ~0.005, in order to avoid control and transition from alloy to isoelectronic doping behavior, was surpassed using AlGaAs emitters and GaAs barriers. The peak values of responsivity, quantum efficiency, and the specific detectivity at 9.6 THz and 4.8 K for a bias field of 2.0 kV/cm are 7.3 A/W, 29%, 5.3×10^{11} Jones, respectively. The background-limited infrared photodetector temperature of 20 K with a 60° field of view was observed for a bias field of 0.15 kV/cm. The f_0 could be further reduced toward ~1 THz regime (~300 μm) by adjusting the Al fraction to offset the effect of residual doping, and/or lowering the residual doping in the barrier, effectively lowering the band bending. © *2005 American Institute of Physics*. [DOI: 10.1063/1.1867561]

Although a threshold frequency (f_0) of ~3.3 THz has been realized[1] in heterojunction interfacial work function internal photoemission (HEIWIP) detectors with GaAs emitters and $Al_{0.005}Ga_{0.995}As$ barriers, further extension is restricted by the Al fraction growth accuracy, and the transition from alloy to isoelectronic doping behavior, to $x\geqslant0.005$ in molecular-beam epitaxy (MBE) grown structures. A detector without any Al (i.e., $x=0$) will give rise to a homojunction interfacial work function internal photoemission detector where f_0 was observed to be limited to ~3 THz due to complications associated with doping concentration above 2×10^{19} cm^{-3}.[2] However, a doped $Al_xGa_{1-x}As$ emitter and GaAs barrier HEIWIPs overcome these limits allowing the realization of f_0 down to ~1 THz and lower. Experimental results have shown that the free carrier absorption coefficients in Be-doped $Al_{0.01}Ga_{0.99}As$ is almost the same as GaAs with similar doping density.[3] This promises similar photon absorption probabilities as in previously reported Be-doped GaAs emitter/$Al_xGa_{1-x}As$ barrier HEIWIPs.[4]

The heterojunction in HEIWIPs allows reducing f_0 by tuning the band offset using the Al fraction[1] without increasing the doping density as in homojunction detectors.[5] A low enough doping density maintains a lower dark current,[4] which improves the detectivity. Compared to the Ga-doped Ge detectors[6] currently used in this range, array fabrication will be much easier with HEIWIPs as the application of mechanical stress to individual pixels of the array is not needed. The other major alternative—a bolometer—has a very low response speed (<1000 Hz), while the HEIWIPs have transit-time-limited speeds on the order of GHz for a bias field of 2 kV/cm. The quantum well photodetectors (QWIPs) have recently extended the f_0 to ~5 THz.[7] However, it is still below the response region of HEIWIPs and, in QWIPs, decreasing the frequency further below requires the doping density to be decreased to reduce dark current, but this lowers the absorption and therefore the sensitivity. Recently, a three-terminal device operating at 2.5 THz was reported.[8]

The $Al_{0.005}Ga_{0.995}As$/GaAs HEIWIP detector structure (V0207) was grown by MBE on a semi-insulating (100) GaAs substrate. The structure consists of ten periods of 3×10^{18} cm^{-3} Be-doped 500 Å thick $Al_{0.005}Ga_{0.995}As$ emitter and 2000 Å thick GaAs barrier sandwiched between two contacts. The top and bottom contacts are 1×10^{19} cm^{-3} Be-doped 500 and 7000 Å thick $Al_{0.005}Ga_{0.995}As$ layers, respectively. The sample was processed by delineating square mesa elements of four different areas from 400×400 to $1000\times1000\ \mu m^2$ by wet etching techniques. As the top contact is only 500 Å thick, no etching was done to reduce the thickness, therefore; the top contact was included as a part of the first emitter in calculating hot carrier injection for the model response. This is different from the previous devices which used thicker top contacts, and required a window to be etched for front illumination.[5] The ohmic contacts were formed by deposition of Ti/Pt/Au.

A partial band diagram of the active region of HEIWIPs with an intrinsic barrier is shown in Fig. 1(a). The basic operation[9] is a three-stage process: Free carrier absorption, internal photoemission, and collection of photoemitted carriers. As free carrier absorption involves initial and final energy states within the same continuum, the response of HEIWIPs is inherently broad band and not limited by absorption at longer wavelengths. The zero-response threshold frequency, f_0 is introduced only in the photoemission stage. The internal photoemission of the carriers is characterized by the interfacial work function Δ which corresponds to the energy difference between the bottom of the barrier (for a *p*-HEIWIP) and the Fermi level in the emitter. Therefore, the threshold frequency of the detector $f_0=0.242\Delta$ with f_0 in THz and Δ in meV.

[a)]Also at: NDP Optronics LLC, 236 St. Martins Dr., Mableton, GA; electronic mail: uperera@gsu.edu

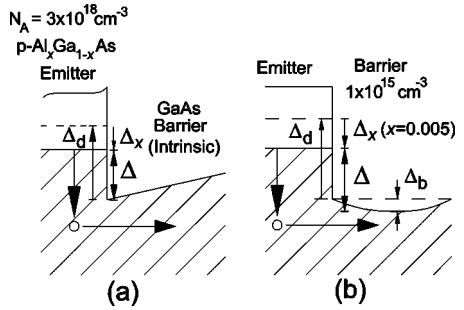

FIG. 1. (a) A partial band diagram of the active region of the HEIWIP device, with an intrinsic barrier under bias showing the contributions to the work function from the band gap narrowing (Δ_d) in the doped emitter and the $Al_xGa_{1-x}As/GaAs$ valance-band offset ($\Delta_x<0$). The dashed line indicates the location of the valence-band edge in the barrier if it were GaAs. Here, $\Delta=\Delta_d+\Delta_x$ where x is the Al fraction. (b) Band bending due to residual doping in the barrier. For zero-bias field, Δ_b is ~13 meV. Since Δ_b is a function of the bias field, for a given bias $\Delta=\Delta_d+\Delta_x+\Delta_b$ and Δ decreases with the bias.

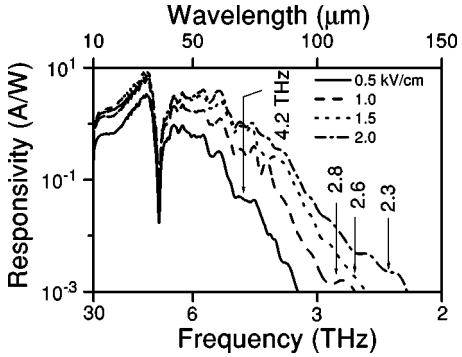

FIG. 3. The variation of responsivity with applied field for sample V0207 at 4.8 K. The peak responsivity, 9 A/W at 9.6 THz, was obtained at 1.5 kV/cm. The increase in response with the field around f_0 is due to threshold shift with the bias. The sharp dip at ~8 THz is due to the interaction of radiation with GaAs-like transverse optical phonons. The bias field decreases the effective work function pushing f_0 toward 2 THz with the increasing field.

For HEIWIPs with intrinsic barriers, Δ has two contributing factors: (i) The band gap offset due to the difference in materials between the emitter and barrier Δ_x, and (ii) the band gap narrowing[10] due to the doping in the emitter layers Δ_d, giving a total $\Delta=\Delta_d+\Delta_x(\Delta_x<0)$ as shown in Fig. 1(a). In the range $N_A\sim1-8\times10^{18}$ cm^{-3}, Δ_d does not vary significantly with doping, while Δ_x can be varied by adjusting the Al fraction of the emitters. However, as shown in Fig. 1(b), bending which originated from the effective residual doping in the barriers could modify Δ such that $\Delta=\Delta_d+\Delta_x+\Delta_b$. The effective doping may be due to the compensation of doping in the barriers. The *n* doping will be fully ionized, while the *p* doping will be only partially ionized, giving a net positive doping. For an unbiased detector, $\Delta_b\simeq13$ meV for a residual doping of 1.1×10^{15} cm^{-3}. Since Δ_b decreases with the bias field, f_0 can be tailored with the ideal minimum corresponding to an intrinsic barrier.

Dark and background photocurrent (300 K with a 60° field of view at the cold stop) of the devices were measured using a Keithly source meter with the sample mounted on the cold finger of a liquid He flow cryostat. The spectral response was measured with 4 cm^{-1} resolution using a Perkin–Elmer system 2000 Fourier-transform infrared spectrometer with a Si composite bolometer as the reference. An SR-785 two-channel fast Fourier transform signal analyzer coupled to a SR-560 high impedance low-noise voltage preamplifier was used for noise density measurements with the sample immersed in liquid He. Intrinsic dark noise levels of the detector were found by measuring four noise current components as in Ref. 11.

The dark current at different temperatures were used to obtain Δ through Arrhenius plots. The variation of Δ with the bias field for three devices with different electrical areas are shown in Fig. 2. The uniform work function is an advantage for detector arrays in terms of spectral shape and detectivity. The Δ at zero bias is ~17 meV for all the mesas decreasing to 10.5 meV at 2 kV/cm. This strong bias dependence is a signature for the presence of residual doping in the barriers.[12] A residual doping of 1.1×10^{15} cm^{-3} was estimated from the Be counts of secondary ion mass spectrometry (SIMS). The small periodic spikes seen on the curves may be due to resonant tunneling through defects in the structure. This is possible because of the low temperature maintained during the

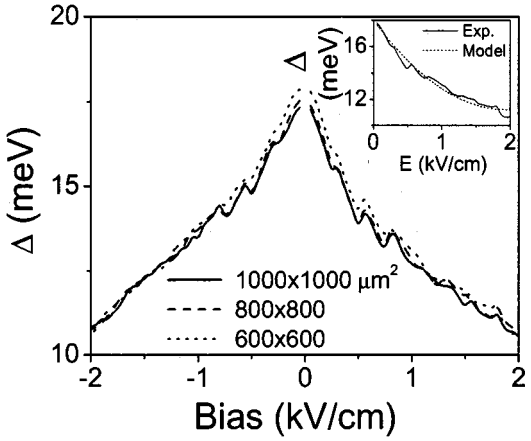

FIG. 2. Variation of work function, Δ with the bias field for three mesas with different electrical areas. The work function at different bias fields were obtained using Arrhenius plots. The zero-bias work function is ~17 meV for all the mesas. Inset shows the experimental and model variations of barrier height for the device with 1000×1000 μm^2 electrical area. The variation with the bias is due to the band bending caused by space charge in the barrier.

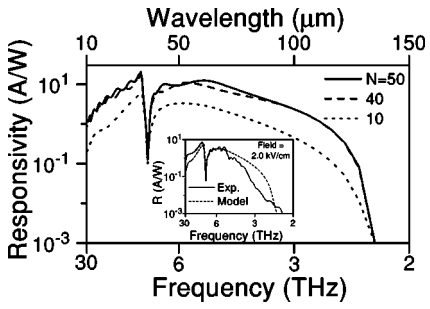

FIG. 4. Calculated responsivity spectra for structures with similar parameters as in V0207 and emitter/barrier periods of $N=10$, 40, and 50 are shown. The responsivities are for a bias field of ~2.0 kV/cm. The detector V0207 is not cavity optimized, while the model structures with $N=40$ and 50 are optimized for 5.6 and 4.9 THz. The cavity peaks of order 3,7,9… are seen while order 5 (7.7 THz) falls in the reststrahlen band of GaAs. The inset shows the experimental responsivity of detector V0207 for a bias field of 2 kV/cm with the calculated responsivity with an optical gain of 2. The arrows indicate the cavity peaks of the detector. The shoulder at 14 μm on both the experimental and the model curves corresponds to the third-order cavity peak while the first order (7.3 THz) falls in the reststrahlen band of GaAs.

TABLE I. Variation of threshold wavelength and frequency with the applied bias field for detector V0207. The increasing field decreases the band bending in the barrier which decreases the threshold frequency.

Bias field (kV/cm)	λ_0 (μm)	f_0 (THz)	R_P (A/W)	η_P (%)	D_P^* (Jones)	D_{Shot} (Jones)
0.5	71.2±0.3	4.21±0.02	3.4	13	⋯	⋯
1.0	108.1±0.6	2.77±0.02	6.3	25	⋯	⋯
1.5	115±6	2.6±0.1	9.0	36	1.5×10^{13}	1.7×10^{13}
2.0	128±9	2.3±0.2	7.3	29	5.3×10^{11}	1.5×10^{12}

growth to minimize the expected Be diffusion.

The variation of responsivity with the bias field at 4.8 K is shown in Fig. 3. For frequencies >6 THz, the responsivity increases with the field with a maximum of 9 A/W at 1.5 kV/cm. Although a further increase in the field would decrease the higher-frequency response, the lower-frequency (<6 THz) response increases due to the reduction in band bending, hence Δ with the field (see Fig. 2). As expected, Δ_b decreases with the field, increasing the threshold to 2.3 THz for a bias field of 2.0 kV/cm. The semilog scale of Fig. 3 clearly shows the variation of f_0 with the applied field. Although further reduction in f_0 was expected with increasing bias, the increasing noise floor of the detector limits it to 2.3 THz. The threshold frequencies along with the figures of merit for different bias fields are shown in Table I. The threshold frequency was obtained using the mean of multiple measurements and the noise floor under dark condition for the given bias field. For f_0=2.3 THz, the best performance of the detector is at 9.6 THz (31 μm), where the responsivity, quantum efficiency, and dark current-limited specific detectivity are 7.3 A/W, 29% and 5.3×10^{11} Jones, respectively.

A dark current-limited peak detectivity of 1.5×10^{13} Jones, which is close to the shot noise limit, was obtained at the bias field of 1.5 kV/cm at 4.2 K. Since the differential resistance of the detector at bias fields <1.5 kV/cm is in the range of several giga ohms, determination of the intrinsic noise level of the detector is beyond our instruments limit. At very high impedance, the measured noise was limited by the Johnson level of the load resistor. A background-limited infrared photodetector temperature of 20 K for a 0.15 kV/cm bias field was recorded.

Model responsivity spectra for V0207(N=10) and two similar structures with different emitter/barrier periods, N =40 and 50, are shown in Fig. 4. The first-order cavity for these structures are at 5.5 and 4.9 THz, respectively. As the total thickness of the detector increases higher-order cavity peaks at higher frequencies start appearing in the responsivity spectra. The model response for N=50 shows the cavity peaks of orders 3,7,9,… while the order 5 falls in the reststrahlen band of GaAs.[13] A band bending contribution of Δ_b=3 meV corresponding to a residual doping of 1.1×10^{15} cm^{-3} in the barrier and a bias field of ~2 kV/cm was considered in the model. Although the overall response improves with increasing N, responsivity below ~3 THz does not increase for N>40. For the structure with N=40, the first cavity peak is at 5.5 THz, giving a responsivity >10 A/W (quantum efficiency, η>25%) at 6 THz and 2.4 A/W (η =3%) at 3 THz.

The inset to Fig. 4 shows experimental responsivity curve for 2.0 kV/cm bias field along with the model (N =10). The best fit to the experimental response for 2.0 kV/cm yields an optical gain of 2. The two arrows indicate the positions of cavity peaks, the shoulder at 21.4 THz is caused by the third-order cavity peak while the first order at 7.3 THz falls in the reststrahlen band. Reflection measurement performed on a piece from the same wafer as V0207 detector showed higher-order cavity peaks above 30 THz. The other small peaks throughout the experimental curve are due to the 620 μm thick substrate interference effect, which is not considered in the model.

In conclusion, an AlGaAs emitter HEIWIP detector with a threshold frequency of 2.3 THz (wavelength of 128 μm) was demonstrated. The threshold can be increased further by compensating the band bending with the emitter Al fraction. AlGaAs emitter GaAs barrier devices will be grown considering this effect to increase the detector threshold close to ~1 THz region.

This work was supported in part by the NSF under Grant No. ECS-0140434 and NASA under SBIR Contract No. NNC04CA95C. One of the authors (M.B.M.R.) is supported by GSU RPE funds. The authors thank I. Sproul for SIMS measurements, and M. Byloos, P. Chow-Chong, R. Dudek, and P. Marshall for microfabrication and packaging.

[1] S. G. Matsik, M. B. M. Rinzan, A. G. U. Perera, H. C. Liu, Z. R. Wasilewski, and M. Buchanan, Appl. Phys. Lett. **82**, 139 (2003).
[2] A. G. U. Perera, S. G. Matsik, M. B. M. Rinzan, A. Weerasekara, M. Alevli, H. C. Liu, M. Buchanan, B. Zvonkov, and V. Gavrilenko, Infrared Phys. Technol. **44**, 347 (2003).
[3] M. B. M. Rinzan, D. G. Esaev, A. G. U. Perera, S. G. Matsik, G. Von Winckel, A. Stintz, and S. Krishna, Appl. Phys. Lett. **85**, 5236 (2004).
[4] A. G. U. Perera, S. G. Matsik, B. Yaldiz, H. C. Liu, A. Shen, M. Gao, Z. R. Wasilewski, and M. Buchanan, Appl. Phys. Lett. **78**, 2241 (2001).
[5] A. G. U. Perera, H. X. Yuan, S. K. Gamage, W. Z. Shen, M. H. Francombe, H. C. Liu, M. Buchanan, and W. J. Schaff, J. Appl. Phys. **81**, 3316 (1997).
[6] E. E. Haller, Infrared Phys. **35**, 127 (1994).
[7] H. C. Liu, C. Y. Song, A. J. SpringThorpe, and J. C. Cao, Appl. Phys. Lett. **84**, 4068 (2004).
[8] J.-Q. Lü, M. S. Shur, J. L. Hesler, L. Sun, and R. Weikle, IEEE Electron Device Lett. **19**, 373 (1998).
[9] D. G. Esaev, M. B. M. Rinzan, S. G. Matsik, and A. G. U. Perera, J. Appl. Phys. **96**, 4588 (2004).
[10] S. C. Jain and D. J. Roulston, Solid-State Electron. **34**, 453 (1991).
[11] A. Van der Ziel, *Noise in Solid State Devices and Circuits* (Wiley-Interscience, New York, 1986).
[12] R. Mosca, P. Bussei, S. Franchi, P. Frigeri, E. Gombia, A. Carnera, and M. Peroni, J. Appl. Phys. **93**, 9709 (2003).
[13] S. Adachi, *GaAs and Related Materials* (World Scientific, Singapore, 1994).